Study of the SiO2-to-Si3N4 etch selectivity mechanism in inductively coupled fluorocarbon plasmas and a comparison with the SiO2-to-Si

Study of the SiO_2-to-Si_3N_4 etch selectivity mechanism in inductively coupled fluorocarbon plasmas and a comparison with the SiO_2-to-Si mechanism

M. Schaepkens, T. E. F. M. Standaert, N. R. Rueger, P. G. M. Sebel,[a] and G. S. Oehrlein[b]
Department of Physics, University at Albany, State University of New York, Albany, New York 12222

J. M. Cook
Lam Research Corporation, Fremont, California 94538-6470

(Received 21 July 1998; accepted 2 October 1998)

The mechanisms underlying selective etching of a SiO_2 layer over a Si or Si_3N_4 underlayer, a process of vital importance to modern integrated circuit fabrication technology, has been studied. Selective etching of SiO_2-to-Si_3N_4 in various inductively coupled fluorocarbon plasmas (CHF_3, C_2F_6/C_3F_6, and C_3F_6/H_2) was performed, and the results compared to selective SiO_2-to-Si etching. A fluorocarbon film is present on the surfaces of all investigated substrate materials during steady state etching conditions. A general trend is that the substrate etch rate is inversely proportional to the thickness of this fluorocarbon film. Oxide substrates are covered with a thin fluorocarbon film (<1.5 nm) during steady-state etching and at sufficiently high self-bias voltages, the oxide etch rates are found to be roughly independent of the feedgas chemistry. The fluorocarbon film thicknesses on silicon, on the other hand, are strongly dependent on the feedgas chemistry and range from ~ 2 to ~ 7 nm in the investigated process regime. The fluorocarbon film thickness on nitride is found to be intermediate between the oxide and silicon cases. The fluorocarbon film thicknesses on nitride range from ~ 1 to ~ 4 nm and the etch rates appear to be dependent on the feedgas chemistry only for specific conditions. The differences in etching behavior of SiO_2, Si_3N_4, and Si are suggested to be related to a substrate-specific ability to consume carbon during etching reactions. Carbon consumption affects the balance between fluorocarbon deposition and fluorocarbon etching, which controls the fluorocarbon steady-state thickness and ultimately the substrate etching. © *1999 American Vacuum Society.* [S0734-2101(99)03201-7]

I. INTRODUCTION

Etching of via or contact holes into SiO_2 to make electrical contact with an underlayer is an indispensable process in modern integrated circuit fabrication technology. High SiO_2 etch rate and selectivity of SiO_2-to-Si are important requirements for etch processes to be commercially viable in manufacturing. Etch processes employing fluorocarbon discharges are typically able to meet these demands, as first reported by Heinecke[1] and an extensive number of subsequent studies.[2–12]

It is believed that the primary mechanism for highly selective SiO_2-to-Si etching using fluorocarbon plasmas is the selective formation of a relatively thick passivating film on the Si surface during steady-state etching conditions. The Si etch rate in that situation is limited by the arrival of atomic fluorine that needs to diffuse through the film to the Si surface, where it chemically reacts.[13–16] For the same process conditions SiO_2 surfaces stay clean of fluorocarbon material, and are etched directly through a mechanism of chemical sputtering.[6,17,18]

The ability to achieve selective etching of SiO_2 over Si_3N_4 is becoming an increasingly important requirement. Silicon nitride is used as a passivating layer that protects circuits from mechanical and chemical attack, or as an etch stop layer, enabling the fabrication of certain damascene and self-aligned contact (SAC) structures. Selective SiO_2-to-Si_3N_4 etching has been demonstrated in several systems.[19–24] Correlations between the Si_3N_4 etch rate and the amount of fluorocarbon material present on the surface during etching suggest a SiO_2-to-Si_3N_4 selectivity mechanism that is analogous to the SiO_2-to-Si etching mechanism. A detailed comparison between the two mechanisms, however, is lacking.

This work summarizes results obtained in a study where SiO_2, Si_3N_4 and Si were processed in an inductively coupled plasma source fed with various fluorocarbon feedgas chemistries (CHF_3, C_2F_6/C_3F_6 and C_3F_6/H_2). Etch rates of SiO_2, Si_3N_4, and poly-Si samples and surface modifications of crystalline Si samples were measured using *in situ* ellipsometry. The surface chemistry of processed SiO_2 and Si_3N_4 samples was examined using postplasma *in situ* x-ray photoelectron spectroscopy (XPS). The experimental results allow a direct comparison of SiO_2, Si_3N_4, and Si etch mechanisms and therefore a comparison of the SiO_2-to-Si_3N_4 and SiO_2-to-Si etch selectivity mechanisms. From this comparison it can be understood why certain feedgas chemistries that give SiO_2-to-Si selectivity do not necessarily give SiO_2-to-Si_3N_4 selectivity. However, it has been found that SiO_2-to-

[a]On leave from Eindhoven University of Technology.
[b]Electronic mail: oehrlein@csc.albany.edu

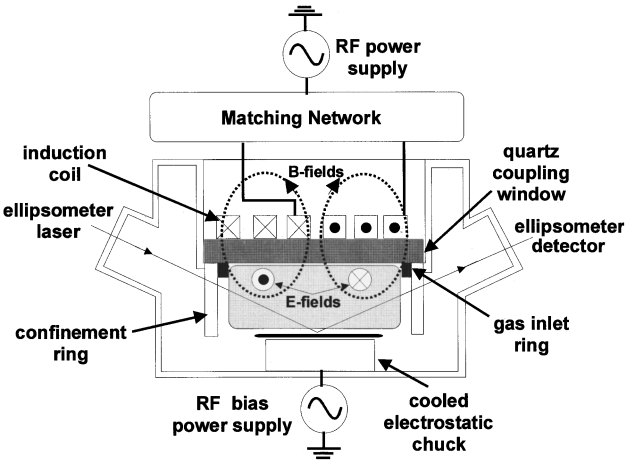

FIG. 1. Schematic outline of the experimental setup of the used ICP source.

Si_3N_4 selectivity in an etching process also provides SiO_2-to-Si selectivity. More importantly, a trend in the etch rate behavior of the different materials has been identified allowing a general description of fluorocarbon plasma etching to be formulated.

II. EXPERIMENTAL SETUP

The high-density plasma source used in this work is a radio-frequency inductively coupled plasma (ICP) source of planar coil design. This plasma source has also been referred to in the literature as transformer coupled plasma (TCP)[25] and radio frequency induction (RFI)[26] source. A schematic outline of the used ICP reactor is shown in Fig. 1. It is similar to the one described by Keller *et al.*[27]

The apparatus consists of an ultrahigh vacuum (UHV) compatible processing chamber in which the plasma source and a wafer holding electrostatic chuck are located. The center part of the ICP source is a planar, 160-mm-diam induction coil that is separated from the process chamber by a 19.6-mm-thick, 230-mm-diam quartz window. The coil is powered through a matching network by a 13.56 MHz, 0–2000 W power supply.

Wafers with a diameter of 125 mm can be placed on a bipolar electrostatic chuck during processing. The chuck is located at a distance of 7 cm downstream from the ICP source and allows the wafer to be rf biased and cooled during processing. A helium pressure of 5 Torr is applied to the backside of the wafer during the experiment to achieve good thermal conduction between the wafer and the chuck.[28] The chuck is cooled by circulation of a cooling liquid.

Samples placed at the center of a wafer can be monitored by an *in situ* He–Ne (632.8 nm) rotating compensator ellipsometer (RCE) in a polarizer-compensator-sample-analyzer (PCSA) configuration. Plasma diagnostics like a retractable Langmuir probe and optical emission spectroscopy (OES) can be used for plasma gas-phase characterization. With the retractable Langmuir probe it is possible to make a scan of the ion current density over 70% of the wafer at a distance of 2 cm above the wafer surface.

A variable frequency rf power supply (500 kHz–40 MHz, 0–300 W) is used to bias the wafer for etching experiments. The experiments reported in this work were all performed at 3.4 MHz. In the process regime investigated, no significant influence of rf biasing on the ion current density measured with the Langmuir probe was observed. The ion energy and the ion flux to the surfaces can thus be varied independently.

The process chamber is pumped using a 450 l/s turbomolecular pump backed by a roughing pumpstack, consisting of a roots blower and a mechanical pump. The process gases are admitted into the reactor through a gas inlet ring located just under the quartz window. The pressure is measured with a capacitance manometer. Pressure control is achieved by an automatic throttle valve in the pump line.

In order to remove deposited fluorocarbon films from the walls of the process chamber, the chamber is cleaned with an O_2 plasma after each experiment. The cleaning process is monitored by taking real time OES data. The absence of optical emission of fluorocarbon related gas phase species is a measure for the cleanliness of the chamber.

The ICP apparatus is connected to a wafer handling cluster system. Processed samples were transported under UHV conditions to a Vacuum Generators ESCA Mk II surface analysis chamber for x-ray photoelectron spectroscopy (XPS) analysis using a polychromatic Mg $K\alpha$ x-ray source (1253.6 eV). Photoelectron spectra were obtained at photoemission angles of 90° and 15° with respect to the sample surface.

III. EXPERIMENTAL RESULTS

A. Fluorocarbon deposition and etch rates

In fluorocarbon plasma processing, deposition and etching occur simultaneously. Deposition and etching processes have different dependencies on the energy of the ions that bombard the surface on which they occur. By varying the ion bombardment energy one can therefore switch from fluorocarbon deposition to etching of earlier deposited fluorocarbon material or other substrate materials, such as SiO_2, Si_3N_4, or Si.

At low self-bias voltages, i.e., low ion bombardment energy, these processes produce net fluorocarbon deposition. The deposition characteristics are strongly dependent on the feedgas chemistry. Figure 2(a) shows the fluorocarbon deposition rates obtained as a function of feedgas (CHF_3, C_2F_6, C_3F_6, and C_3F_6/H_2) in discharges at 6 mTorr operating pressure, 1400 W inductive power, and no rf bias power applied to the surface. The deposition rate in CHF_3 and C_2F_6 is significantly lower than in C_3F_6 or C_3F_6/H_2. The highly polymerizing character of C_3F_6 or C_3F_6/H_2 discharges may be related to the size and chemical structure of the fluorocarbon parent molecules.[2,24]

Figure 2(b) shows the refractive index of the deposited fluorocarbon films using the different gases. The refractive index of the fluorocarbon deposited using C_2F_6 and C_3F_6 are found to be lower than if CHF_3 or C_3F_6/H_2 is used. Crystalline Si samples on which 150 nm fluorocarbon material was deposited were analyzed by XPS. It was found that the

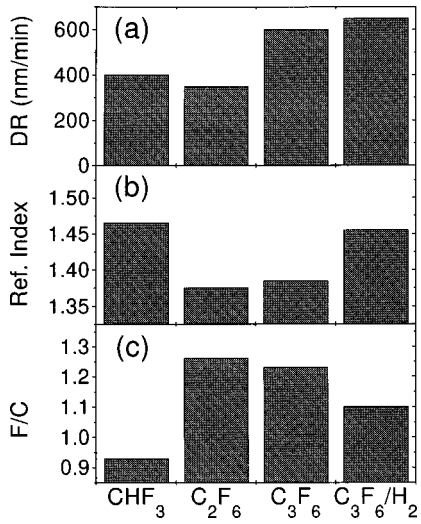

FIG. 2. (a) Deposition rates, (b) refractive index, and (c) fluorine-to-carbon ratio determined from XPS analysis of fluorocarbon material deposited at 6 mTorr operating pressure in discharges fed with 40 sccm of CHF_3, C_2F_6, C_3F_6, or C_3F_6/H_2 (27%). The fluorine-to-carbon ratios determined under 15° electron escape angle are slightly higher than the ratio determined under 90°. The values in (c) are averages of the two values.

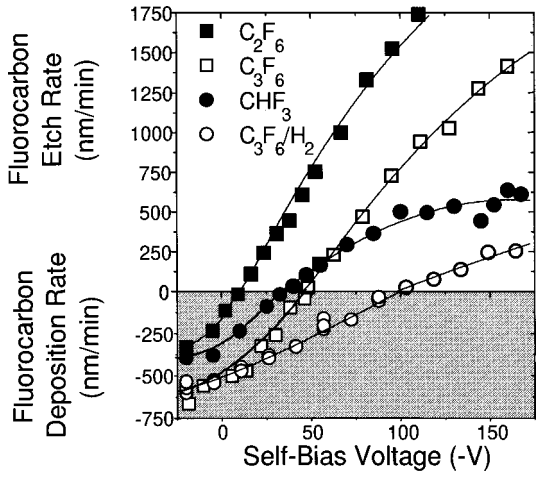

FIG. 3. Fluorocarbon etch rates as a function of self-bias voltage, measured with respect to ground, at 6 mTorr operating pressure in discharges fed with 40 sccm of CHF_3, C_2F_6, C_3F_6, or C_3F_6/H_2 (27%). The fluorocarbon substrate was deposited at 0 W rf bias power at the same process condition where the etch rates were determined. The plasma potential at these conditions typically varies between 20 and 30 V. This potential needs to be added to the self-bias voltage in order to estimate the actual average ion bombardment energy.

fluorine-to-carbon ratio of the fluorocarbon material, see Fig. 2(c), is inversely proportional to the refractive index. Further, the fluorine-to-carbon ratio of the deposited fluorocarbon material is lower if hydrogen is present in the feedgas chemistry. This trend can be explained by the fluorine scavenging effect of hydrogen in the gas phase,[2] or more likely at these operating pressures fluorine reduction as a result of hydrogen–fluorine recombination at the reactor walls. Also, fluorine abstraction by hydrogen from a fluorocarbon surface could explain the observations.[29]

The fluorocarbon films that deposit if no bias is applied to the substrate, can be etched off the thin film substrate at self-bias voltages above a certain threshold value. The etch rates of the fluorocarbon films deposited at unbiased conditions have been measured as a function of self-bias voltage by *in situ* ellipsometry in discharges of CHF_3, C_2F_6, C_3F_6, and C_3F_6/H_2 at 6 mTorr operating pressure and 1400 W inductive power. The fluorocarbon etch rates are plotted as positive values in Fig. 3. Also included in Fig. 3 are the fluorocarbon deposition rates (negative values) measured by *in situ* ellipsometry at self-bias voltages below the threshold for etching. It shows that the fluorocarbon deposition rate decreases as the self-bias voltage increases.

The fluorocarbon etch rates are found to be strongly dependent on the feedgas chemistry. First, the fluorocarbon etch rate is relatively low at conditions where hydrogen is present in the feedgas mixture, e.g., compare CHF_3 to C_2F_6 processing and C_3F_6 to C_3F_6/H_2 processing. This observation can be attributed to the fact that fluorine is a precursor for etching of fluorocarbon material.[3] The presence of hydrogen in the feedgas chemistry namely results in (a) a reduction of fluorine in the plasma gas phase (observed when comparing optical emission spectra from 40 sccm CF_4 and 40 sccm CHF_3 plasmas at identical conditions), and (b) a more fluorine depleted fluorocarbon substrate (the fluorine-to-carbon ratio of fluorocarbon is reduced, see Fig. 2). A second observation is that the higher the fluorocarbon deposition rate at 0 W bias power, the lower the fluorocarbon etch rate under biased conditions, e.g., compare C_2F_6 to C_3F_6 processing and CHF_3 to C_3F_6/H_2 processing. Net fluorocarbon etching apparently benefits from a reduction in fluorocarbon deposition.

The position of the threshold voltage for net etching is consistent with the above observations. If hydrogen is present in the feedgas chemistry or if the fluorocarbon deposition rate at 0 W bias power is high, the threshold voltage is relatively high, and vice versa.

B. SiO_2, Si_3N_4, and Si etch rates

At conditions where net fluorocarbon etching takes place, other substrate materials, such as SiO_2, Si_3N_4, and Si, can also be etched. Figure 4 shows the SiO_2, Si_3N_4, and Si etch rates measured on blanket samples by *in situ* ellipsometry as a function of self-bias voltage in discharges of CHF_3, C_2F_6, C_3F_6, and C_3F_6/H_2 at 6 mTorr operating pressure and 1400 W inductive power.

At sufficiently high self-bias voltage, SiO_2 etching of the blanket samples occurs at a relatively high rate, which is roughly independent of the feedgas chemistry. This is consistent with Langmuir probe measurements performed for the different discharges. The Langmuir probe data showed that the ion current density does not vary significantly with feedgas chemistry. Since SiO_2 etching has been suggested to occur through a chemical sputtering mechanism in which the ion flux is the limiting factor,[18] the SiO_2 etch rate is expected to be relatively independent of the feedgas chemistry. (Note: this is the case if the average composition of the fluorocar-

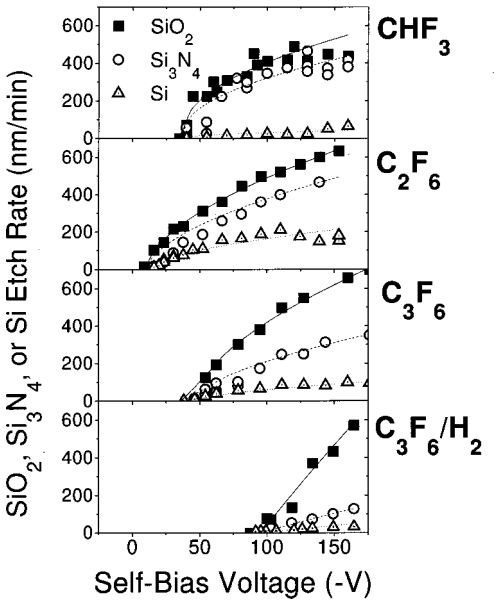

FIG. 4. Etch rates of SiO_2, Si_3N_4, and Si substrates as a function of self-bias voltage at 6 mTorr operating pressure in discharges fed with 40 sccm of CHF_3, C_2F_6, C_3F_6, or C_3F_6/H_2 (27%).

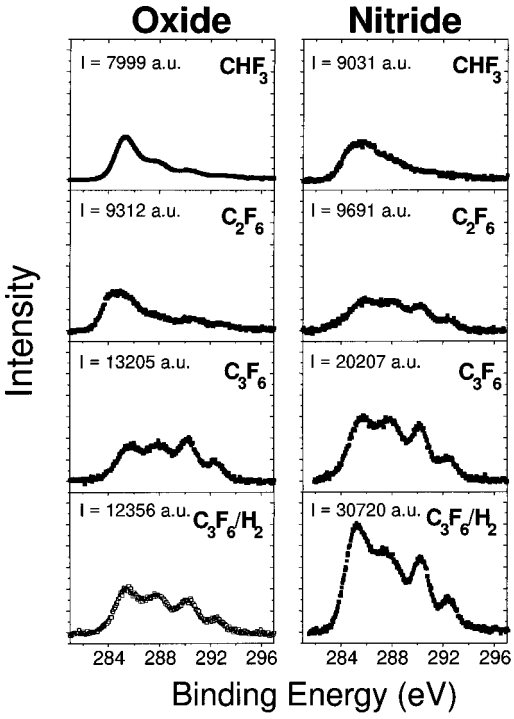

FIG. 5. C(1*s*) spectra obtained by XPS surface analysis under 90° emission angle on SiO_2 and Si_3N_4 samples processed in CHF_3 (40 sccm), C_2F_6 (40 sccm), C_3F_6 (40 sccm), and C_3F_6/H_2 (20 sccm/15 sccm) discharges at 6 mTorr and a self-bias voltage of −100 V. The C (1*s*) intensity is a measure for the amount of fluorocarbon material present on the surfaces during steady-state etching conditions.

bon ion flux that bombards the SiO_2 surface does not change significantly with the various conditions. If the average composition of the ion flux changes, e.g., from CF_2^+ to CF^+, the average SiO_2 sputter yield possibly changes as well.)

The blanket Si etch rates for the above conditions are significantly lower than the SiO_2 etch rates. The etch rates of silicon show a strong dependence on feedgas chemistry. The dependence is similar to that observed for fluorocarbon etching, suggesting that the effects due to hydrogen addition and fluorocarbon deposition rate ultimately are also responsible for the etch rate behavior of Si.

Etching of Si_3N_4 is intermediate between SiO_2 and Si, both in etch rate and dependence on the feedgas chemistry. For chemistries that result in a low fluorocarbon deposition rate, the Si_3N_4 etch rate is relatively independent of the feedgas, similar to SiO_2 etching. For chemistries resulting in a high fluorocarbon deposition rate, the Si_3N_4 etch rate dependence is similar to that observed for Si and fluorocarbon etching. In other words, hydrogen addition only helps to suppress Si_3N_4 etching at conditions where the fluorocarbon deposition rate is sufficiently high.

C. Surface analysis: Steady-state fluorocarbon films

The surface chemistry of processed SiO_2 and Si_3N_4 samples was investigated by XPS as a function feedgas chemistry in discharges at 6 and 20 mTorr operating pressure. The feedgas chemistries used were CHF_3, C_2F_6, C_3F_6, and mixtures of C_2F_6/C_3F_6 and C_3F_6/H_2. At the same conditions the surface modifications of crystalline Si samples were measured by *in situ* ellipsometry.[30]

Figure 5 shows high-resolution C (1*s*) photoemission spectra obtained from SiO_2 and Si_3N_4 surfaces etched at −100 V self-bias voltage at 6 mTorr operating pressure in discharges fed with CHF_3, C_2F_6, C_3F_6, and C_3F_6/H_2. The binding energies were corrected for charging of the dielectric substrate materials. The integrated intensity of the C (1*s*) spectrum, plotted in the upper left corner of each graph in Fig. 5, is a measure for the amount of fluorocarbon material present on the sample surface. It shows that the C (1*s*) intensity from processed SiO_2 surfaces is typically lower than the intensities measured on Si_3N_4 samples processed under the same process conditions, and compared to processed Si_3N_4 samples relatively independent of the feedgas chemistry. The intensity of the C (1*s*) spectrum from processed Si_3N_4 depends significantly on the feedgas chemistry. It clearly shows that the amount of fluorocarbon material on the Si_3N_4 surface shown in Fig. 5, is inversely proportional to the corresponding etch rate at −100 V self-bias from Fig. 4.

The C (1*s*) intensity measured on the processed surfaces can be expressed as a fluorocarbon film thickness. This thickness can be calculated from photoemission intensities, due to the exponential decay of the XPS signal with depth. A method that uses angular resolved intensities from substrate elements is described by Rueger *et al.*[18] Standaert *et al.*[16] describe a method of quantifying the fluorocarbon film thickness by comparing the C (1*s*) intensity from a processed sample to the C (1*s*) intensity of a semi-infinitely thick fluorocarbon film (e.g., a fluorocarbon film deposited at 0 W). A comparison of the two methods showed that at low C (1*s*) intensities, both methods give very similar values for the fluorocarbon thickness. At high C (1*s*) intensities, slightly

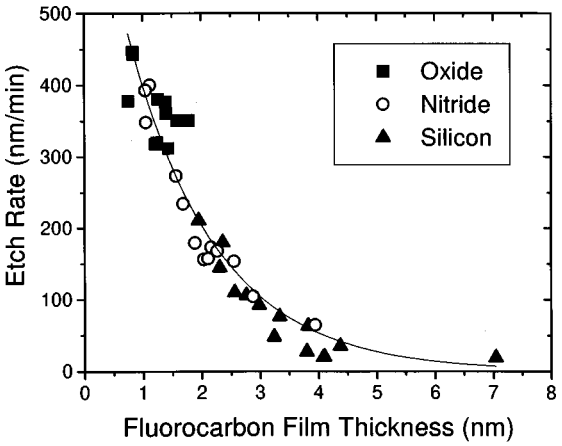

FIG. 6. Etch rates of SiO_2, Si_3N_4, and Si samples plotted vs the thickness of the fluorocarbon film present on the surface during steady-state etching conditions. The varying parameters are feedgas chemistry [CHF_3 (40 sccm), C_2F_6 (40 sccm), C_3F_6 (40 sccm), and C_3F_6/H_2 (20 sccm/15 sccm)] and operating pressure (6 and 20 mTorr). The rf bias power level corresponded to a self-bias voltage of -100 V. It clearly shows that the thicker the fluorocarbon film, the lower the etch rate.

higher values for the fluorocarbon film thickness are found with the latter method. The discrepancy between the two methods results from the fact that the error in the determination of the thickness in both methods increases as the amount of fluorocarbon material on the surface increases. In this work the average of the thicknesses determined by the two methods is used to quantify the fluorocarbon film thickness. In Fig. 6 the etch rates of SiO_2 and Si_3N_4 are plotted as a function of the fluorocarbon film thickness for all investigated chemistries (CHF_3, C_2F_6/C_3F_6, and C_3F_6/H_2) and pressures (6 and 20 mTorr) obtained at -100 V self-bias. Data for silicon etched at the same conditions as SiO_2 and Si_3N_4 is also included. The film thicknesses on silicon were determined in real time by *in situ* He–Ne ellipsometry. In the conversion from ellipsometric angles Ψ and Δ to fluorocarbon film thickness, it is assumed that the steady-state fluorocarbon film has the same refractive index as fluorocarbon deposited at the same process conditions without rf bias applied. This assumption is supported by XPS analysis,[16] which indicates that the composition of the steady-state fluorocarbon films and passively deposited fluorocarbon material does not vary significantly.

Figure 6 clearly shows a general trend for the investigated process regime; i.e., the etch rate of a thin film material decreases with increasing thickness of the steady-state fluorocarbon film on its surface. It can be seen that independent of the process conditions the SiO_2 surfaces stay relatively clean of fluorocarbon material (fluorocarbon film thickness$\leqslant$1.5 nm). The ion penetration depth in the investigated energy range is around 1 nm.[31] The SiO_2 surfaces can thus be etched directly by a mechanism of chemical sputtering,[6,17,18] which explains the relatively high etch rate. The Si surfaces are covered with a fluorocarbon film that is strongly dependent on the process conditions but typically relatively thick (2–7 nm). It is therefore unlikely that direct ion impact contributes to the Si etch rate. Instead, the etch rate is suggested to be limited by the arrival of atomic fluorine at the Si surface. Since the fluorine needs to be transported through the relatively thick fluorocarbon film by a diffusion mechanism;[13–16] the Si etch rates are suppressed. The fluorocarbon films on Si_3N_4 are of intermediate thickness compared to SiO_2 and Si (1.25–3.75 nm). For certain conditions a thick fluorocarbon film is present and the Si_3N_4 etch rate is suppressed, similarly to the Si etch rate. For other conditions the fluorocarbon films are relatively thin, and the Si_3N_4 etch behavior is similar to that of SiO_2.

From Fig. 6 it is clear that SiO_2-to-Si_3N_4 selectivity can be achieved only if a thick enough fluorocarbon film forms on the Si_3N_4 surface, while keeping the SiO_2 surface clean. This is completely analogous to the SiO_2-to-Si selectivity mechanism. However, Fig. 6 also shows that for conditions where Si is already covered with a relatively thick fluorocarbon and the etch rate is suppressed, the fluorocarbon film on Si_3N_4 can be still thin enough for direct chemical sputtering to occur. This explains why a process condition that enables SiO_2-to-Si selectivity does not necessarily allow for SiO_2-to-Si_3N_4 selectivity, while all process conditions enabling SiO_2-to-Si_3N_4 etch selectivity, automatically also provide SiO_2-to-Si selectivity.

D. Surface analysis: Reaction layers

In the previous section it was suggested that in the case that a substrate is covered with a relatively thick steady-state fluorocarbon film, the etch rate is limited by the arrival of atomic fluorine which needs to diffuse towards the substrate surface. This suggestion is based on the observations by Oehrlein *et al.*[1] who found that in the case of Si etching the thickness of a fluorinated silicon reaction layer located under the steady-state fluorocarbon film decreases if the thickness of the fluorocarbon overlayer increases. This observation rules in favor of the fluorocarbon film protecting the Si from fluorine attack, rather than that diffusion of etch products out through the fluorocarbon film would be the rate limiting step (which is also consistent with the etch rate being inversely proportional to the fluorocarbon film thickness).

Based on the observations in Fig. 6, which suggest a general etch mechanism for SiO_2, Si_3N_4, and Si in fluorocarbon plasmas, the presence of a fluorinated oxide or nitride reaction layer is to be expected. To verify the presence of these reaction layers, a detailed analysis of high resolution C (1*s*), F (1*s*), Si (2*p*), and N(1*s*) or O(1*s*), was performed.

The C (1*s*) spectra from Fig. 5 can typically be deconvolved into four different Gaussian peaks corresponding to different chemical carbon bonds (C–CF_n, C–F, C–F_2, and C–F_3), using a least-squares fitting routine and linear background subtraction. In certain cases where the fluorocarbon films are relatively thin and the fluorocarbon–substrate interface is visible to XPS analysis, a C–C/C–Si peak needs to be included for obtaining a proper fit of the C (1*s*) spectrum. The binding energies corresponding to the different carbon bonds are given in Table I. From the deconvolving of the C (1*s*) spectra fluorine-to-carbon ratios F/C_{dec} were calculated as follows:

TABLE I. Listing of photoelectron binding energies.

Element	BE	Specification	Reference
C (1*s*)	283.4 eV	C–C/C–Si	16
	285.5 eV	$C–CF_n$	
	288.0 eV	C–F	
	290.3 eV	$C–F_2$	
	292.6 eV	$C–F_3$	
F (1*s*)	687.1 eV		32
Si (2*p*)	103.4 eV	SiO_2	32
Si (2*p*)	101.7 eV	Si_3N_4	33
O (1*s*)	532.6 eV	SiO_2	33
N (1*s*)	397.5 eV	Si_3N_4	33

$$F/C_{dec}=\frac{I_{C-F}+2\cdot I_{C-F_2}+3\cdot I_{C-F_3}}{I_{C-C/C-Si/C-CF_n}+I_{C-F}+I_{C-F_2}+I_{C-F_3}}, \quad (1)$$

where I_{bond} the photoemission intensity (i.e., area under each Gaussian) originating from a specific bond. The fluorine-to-carbon ratio can also be calculated by dividing the intensity of the F (1*s*) spectrum (BE=687.1 eV)[32] by the total C (1*s*) intensity, after correcting for differences in photoemission crossections. In the rest of this work we will indicate the fluorine-to-carbon ratio calculated in the latter fashion by F(1*s*)/C(1*s*). Figure 7 shows the difference $\Delta F/C$ between the fluorine-to-carbon ratios determined by the two methods, i.e.,

$$\Delta F/C=F(1s)/C(1s)-F/C_{dec}, \quad (2)$$

for both processed SiO_2 and Si_3N_4 surfaces as a function of fluorocarbon film thickness. The XPS analysis was performed at both 15° and 90° photoelectron take off angle. For XPS spectra obtained under 15° photoelectron take off angle, which is a surface sensitive condition, $\Delta F/C$ is close to zero. At 90° photoelectron take off angle $\Delta F/C$ is also close to zero at conditions where a relatively thick fluorocarbon film is present on the substrates. This data thus shows that the F (1*s*) photoelectrons detected from all samples using the 15° take off angle as well as from samples with a relatively thick fluorocarbon film on the surface using the 90° take off angle primarily originate from fluorine bonded to carbon in the fluorocarbon film. If the fluorocarbon film thickness is small, however, the F(1*s*)/C(1*s*) ratio is found to be higher than the F/C_{dec} ratio, resulting in a value for $\Delta F/C$ that is larger than zero. This means that a significant part of the F (1*s*) photoelectrons detected from samples with a relatively thin fluorocarbon film on the surface at 90° take off angle must originate from fluorine species that are not bonded to carbon.

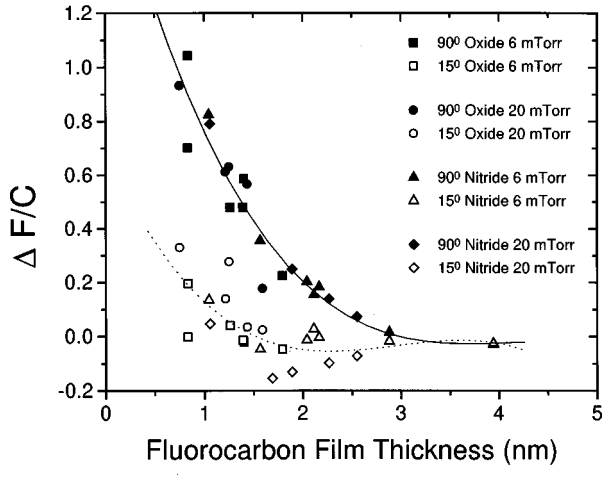

FIG. 7. Difference between the fluorine to carbon ratios determined from F(1*s*)/C(1*s*) and C (1*s*) only, as a function of fluorocarbon film thickness.

The above data suggest that the fluorine that is not bonded to carbon is located underneath the steady-state fluorocarbon film, since it can be detected only if the path of the photoelectrons from the underlayer through the fluorocarbon film is significantly smaller than the electron escape depth (e.g., 90° escape angle and thin fluorocarbon overlayers). The electron escape depth is typically in the order of a few nanometers.

The fluorine that is not bonded to carbon and that is located underneath the fluorocarbon film can be expected to form fluorinated SiO_2 and Si_3N_4 reaction layers. In the case of Si etching, the films could be observed in the high resolution Si (2*p*) XPS spectra. In the case of SiO_2 and Si_3N_4 etching, it is possible to obtain information on the reaction layers from substrate elements, Si (2*p*) and N (1*s*) or O (1*s*).

Indeed, the Si (2*p*) spectra at 15° electron escape angles obtained from processed Si_3N_4 samples were found to be antisymmetric and have been deconvolved into two Gaussian peaks, as shown in Fig. 8(a). The low binding energy peak corresponds to Si (2*p*) in bulk Si_3N_4 [BE=101.7 eV; full width at half maximum (FWHM)=2.3 eV).[33] The high binding energy peak is found to be shifted by 2.1 ± 0.2 eV and has a FWHM of 2.7 ± 0.1 eV. The shift towards a higher binding energy with respect to bulk Si_3N_4 can be explained by silicon bonding to electronegative fluorine. Similarly, the N (1*s*) spectrum taken at glazing angles on processed nitride samples can also be deconvolved in two Gaussians, see Fig. 8(b). The low binding energy peak corresponds to N (1*s*) in bulk Si_3N_4 (BE=397.5 eV; FWHM=2.2 eV).[33] The high binding energy peak is found to be shifted by 2.27 ± 0.35 eV and has a FWHM of 3.00 ± 0.25 eV, and can be attributed to substrate nitrogen bonded to more electronegative elements, such as fluorine or carbon with fluorine neighbors. The observed shift is consistent with this, since (iso)cyanides are reported to have binding energies in the range of 397.5–400.2 eV.[34] The above results are consistent with the existence of a fluorinated Si_3N_4 reaction layer. In the following we will associate the high binding energy peaks with either reacted silicon or nitrogen.

The reacted intensity (Gaussian peak corresponding to reaction with F) divided by the unreacted (Gaussian corresponding to bulk material) intensity is higher under grazing angles than under 90° electron take off angle in both Si (2*p*) and N (1*s*) spectra. This indicates that the fluorinated Si_3N_4 layer is on top of the bulk Si_3N_4 owing to the fact that the sampling depth (measured perpendicular to the surface) at 15° is a factor of sin(15°) smaller than at 90°. Both the reacted and unreacted Si (2*p*) and N (1*s*) intensities decrease

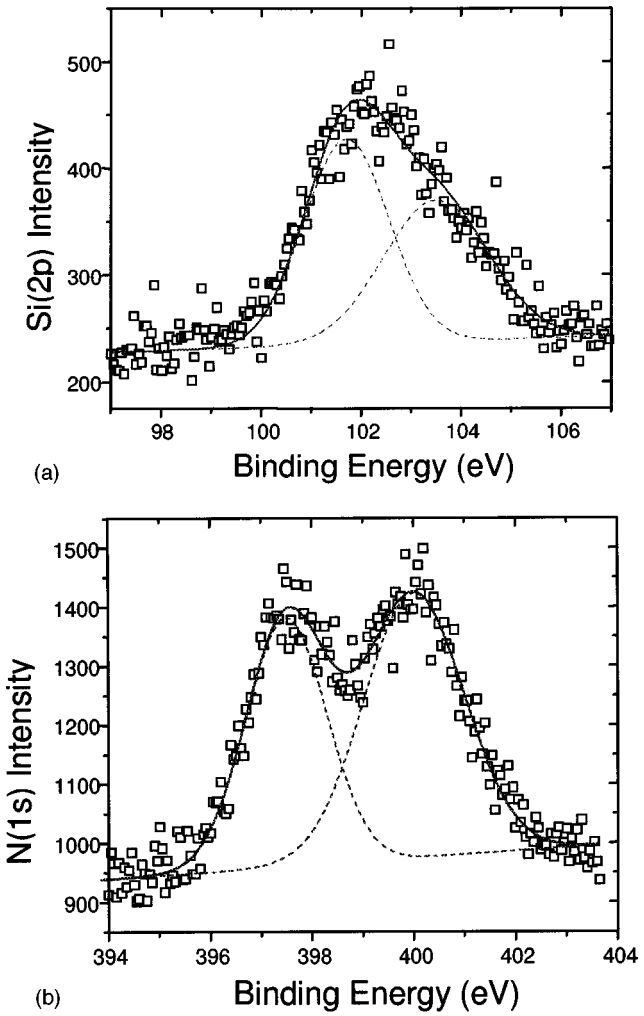

FIG. 8. (a) Typical Si (2*p*) and (b) typical N (1*s*) spectra obtained from a processed Si_3N_4 sample under 15° photoemission angles.

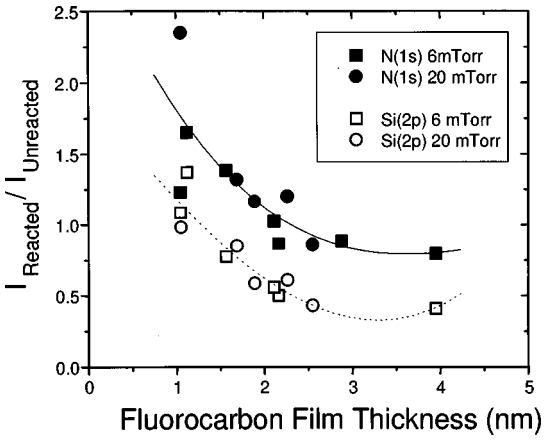

FIG. 9. Ratio of reacted intensity to unreacted intensity as a function of fluorocarbon film thickness for both Si (2*p*) and N (1*s*) signals under 15° photoemission angle.

with increasing fluorocarbon film thickness. This indicates that both the reacted and unreacted Si_3N_4 are located underneath the fluorocarbon material. In other words, the fluorinated Si_3N_4 reaction layer is, again analogous to Si etching, located at the interface between the Si_3N_4 sample and the fluorocarbon film.

The intensity ratio $I_{\text{reacted}}/I_{\text{bulk}}$ of reacted to unreacted Si (2*p*) or N (1*s*) is related to the thickness of the fluorinated Si_3N_4 reaction layer d_{reacted}:[14,35]

$$d_{\text{reacted}} = \lambda \ln\left(1 + \frac{(I_{\text{reacted}}/I_{\text{bulk}})}{K}\right), \tag{3}$$

where λ the photoelectron escape depth and K the ratio of the atomic density of reacted atoms in the reaction layer to the atomic density of unreacted atoms in the bulk Si_3N_4. Since the intensity ratio $I_{\text{reacted}}\, I_{\text{bulk}}$ decreases with fluorocarbon film thickness, see Fig. 9, it can be concluded that the thickness of the fluorinated Si_3N_4 reaction layer decreases as the fluorocarbon film thickness increases, similar to what Oehrlein *et al.*[14] observed for Si etching.

A similar detailed surface analysis was performed in attempt to obtain information on fluorinated SiO_2 reaction layers. However, it was not possible in either the O (1*s*) or the Si (2*p*) spectra to distinguish between intensities origination from a reaction layer or from the bulk SiO_2. This is due to the fact that the binding energies of silicon bonded to fluorine and silicon in bulk SiO_2 are too close to be resolved. Further, it is rather unlikely that fluorine will bond to oxygen. Next to the data in Fig. 7, from which one can expect that part of the Si (2*p*) photoelectrons originate from a fluorinated SiO_2 reaction layer in which fluorine is bonded to substrate silicon, we do not have additional experimental evidence for the existence of such a layer. The formation of a fluorinated SiO_2 has however been observed by various investigators using additional surface analytical techniques.[32,36]

The results presented in this section are consistent with the results in Fig. 6, which suggest a general etch mechanism for SiO_2, Si_3N_4, and Si in fluorocarbon plasmas: the thickness of the steady-state fluorocarbon film controls the formation of a fluorinated reaction layer and thus the etch rate of the various substrates.

IV. DISCUSSION

The experimental results presented in the previous section suggest that a general mechanism exists for SiO_2, Si_3N_4, and Si etching in fluorocarbon plasmas. The formation of the etch rate controlling steady-state fluorocarbon film is therefore key in etch selectivity control. The mechanism for the formation of a steady-state fluorocarbon film and the dependence on substrate chemical composition and feedgas chemistry conditions will be discussed below.

A. Mechanism of fluorocarbon film formation

Initially, after ignition of the plasma, fluorocarbon deposition takes place on the substrate material. The deposited fluorocarbon film will be exposed to ion bombardment when an rf bias is applied. Ion bombardment will result in breaking bonds in the fluorocarbon material and thus in the release of

fluorine, which is an etchant for both fluorocarbon and the investigated substrate materials. It is also possible that free atomic fluorine radicals are produced at the surface due to impact dissociation of fluorocarbon ions. Additionally, the flux of gas phase species to the surface is a possible source for fluorine radicals.

In addition to the production of the etchant fluorine, ion bombardment provides the fluorocarbon/substrate system with energy, which is the a second necessary component for etching of the investigated substrate materials as was shown by Ding *et al.*[37] The energy dissipated in the fluorocarbon material will be attenuated as the ions penetrate deeper into the fluorocarbon film. The energy dissipation combined with the presence of atomic fluorine will result in chemical reactions between atomic fluorine and the fluorocarbon film, i.e., etching of the fluorocarbon material.

When the fluorocarbon film is thin enough, some of the ion bombardment energy will also be dissipated in the substrate material. This energy dissipation in the substrate promotes chemical reactions of fluorine atoms and substrate material, i.e., substrate etching. The total amount of fluorocarbon etched per unit time will be reduced in this case since the available fluorine and energy has to be shared with the substrate etching process. At the point that the fluorocarbon etch and deposition rates balance, steady-state conditions are reached and a steady-state fluorocarbon film is formed on the substrate. The substrate is then being etched with that part of the energy and fluorine that is not required for balancing of the fluorocarbon deposition. The details of how a substrate is etched through a steady-state fluorocarbon film are described by Standaert *et al.*[16] for the case of Si.

In the above mechanism, the etch rate of the substrate material will be reduced if the fluorocarbon deposition rate is increased, since more energy and etch precursors are required for fluorocarbon removal. Similarly, if the fluorocarbon material that is deposited is hard to remove, e.g., due to a reduction in the fluorine content in the deposited material, less energy and etch precursors will be available for net substrate etching. This mechanism, therefore, successfully explains the feedgas chemistry dependence of silicon etching and of Si_3N_4 etching at highly polymerizing conditions. Etching of SiO_2 and Si_3N_4 at low polymerizing conditions, however, was found to be independent of feedgas chemistry. In the following section, the substrate dependence of the etching is explained by the differences in carbon consumption ability of SiO_2, Si_3N_4, and Si substrates. The above mechanism is extended such that it successfully explains this substrate chemistry dependence.

B. Substrate dependence of fluorocarbon film formation

In the above mechanism, fluorocarbon removal is performed only by the plasma. In order to explain the dependence of the steady-state fluorocarbon film thickness on substrate type and the corresponding etch rates of SiO_2, Si_3N_4, and Si, also reactions between the substrate material and fluorocarbon species need to be taken in account. The rate of

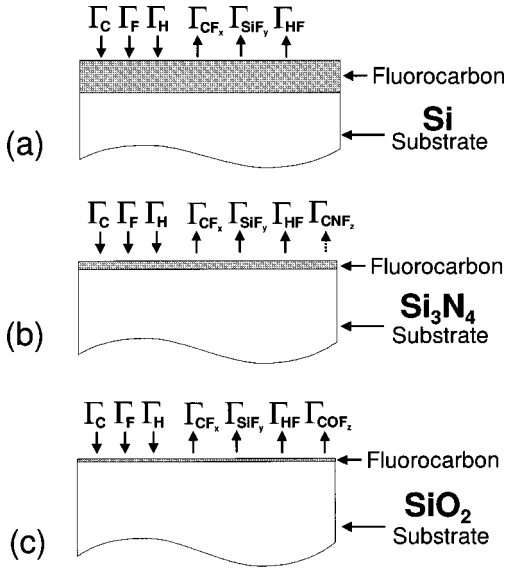

FIG. 10. Schematic view of fluxes incident on and outgoing from the (a) Si, (b) Si_3N_4, and (c) SiO_2 substrates. In the case of Si, no volatile product between the substrate material and carbon exists, and a relatively thick steady-state fluorocarbon film develops. In the case of SiO_2, most of the carbon is consumed in reactions with substrate oxygen, and a relatively thin steady-state fluorocarbon film forms. The Si_3N_4 substrate has a moderate ability to react with carbon, and a steady-state fluorocarbon film of intermediate thickness results.

fluorocarbon consumption by the substrate is different for SiO_2, Si_3N_4, and Si, resulting in different balances between etch and deposition for the various substrates. This is schematically depicted in Fig. 10. The ability of SiO_2 to react with carbon species in the fluorocarbon material is greater than for Si_3N_4 or Si.[2–4,6] In other words, reactions between fluorocarbon and SiO_2 with typical volatile reaction products like CO, CO_2, or COF_2, are more effective than reactions between fluorocarbon and Si_3N_4, resulting in the formation of volatile products such as CNF[38,39] and FCN.[40] The difference in fluorocarbon consumption ability between SiO_2 or Si_3N_4 is possibly due to differences in bond strengths, substrate stoichiometry, volatility of the reaction products, etc. In Si etching there is no volatile carbon containing compound at all that can be formed in reactions of fluorocarbon species and the substrate.

The reactions between fluorocarbon and the SiO_2 substrate results in consumption of the majority of the deposited fluorocarbon material during etching reactions.[18] Fluorocarbon removal by the plasma is therefore not a limiting factor for net substrate etching. Provided that there is enough energy for chemical sputtering, the SiO_2 surfaces will stay relatively clean for any deposition rate or fluorocarbon etch rate. The SiO_2 etch rates will therefore be relatively independent of the feedgas chemistry (provided that the ion current density and the average ion flux composition in the various discharges are comparable). On the other hand in Si etching, where the substrate cannot assist in the carbon removal during etching, fluorocarbon can only be removed by the plasma. The fluorocarbon etch rate is therefore the limiting

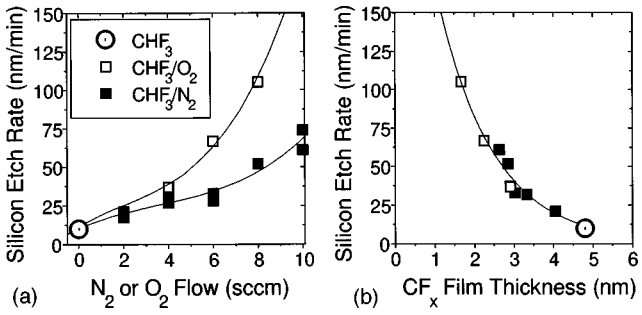

FIG. 11. (a) Silicon etch rates as a function of O_2 and N_2 flow added to a 40 sccm CHF_3 discharge at 7 mTorr at −100 V self-bias. (b) Silicon etch rates as a function of corresponding fluorocarbon film thickness on the silicon surface.

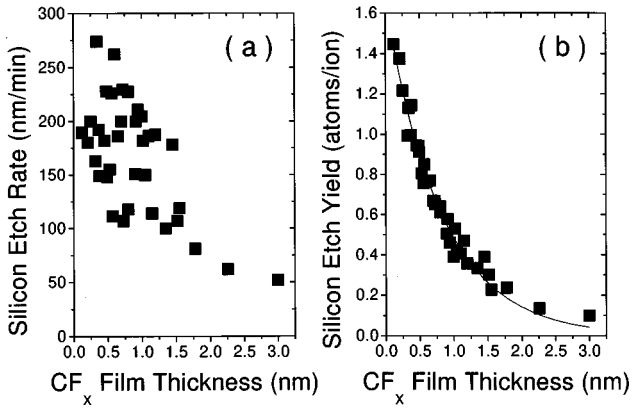

FIG. 12. (a) Silicon etch rates measured in C_2F_6 plasma for a variety of conditions (6–20 mTorr operating pressure, 10–40 sccm gas flow, and 600–1400 W inductive power) at −100 V self-bias as a function corresponding steady-state fluorocarbon film thickness. (b) Etch yields for the same conditions as a function of corresponding fluorocarbon film thickness.

factor, and the Si etch rate will follow the fluorocarbon etch and deposition rate trends as a function of process conditions. Si_3N_4 is intermediate in its ability to consume carbon species during etching. At low fluorocarbon deposition rates, the nitrogen–carbon interaction for a Si_3N_4 substrate is sufficient to maintain a clean surface. The Si_3N_4 etch rate will in this case be independent of the feedgas chemistry. If the fluorocarbon deposition is too high, fluorocarbon removal by the plasma becomes a limiting factor in the Si_3N_4 etching process. The Si_3N_4 etch rate will then follow the fluorocarbon etch and deposition trends.

The suggested role of substrate oxygen and nitrogen in carbon consumption is supported by the results from an experiment in which small amounts of O_2 or N_2 are added to a CHF_3 (40 sccm) discharge, see Fig. 11. The Si etch rates and corresponding fluorocarbon film thicknesses were measured by *in situ* ellipsometry as a function of O_2 and N_2 flow at −100 V self-bias voltage, at 1400 W inductive power and 7 mTorr operating pressure. First, Fig. 11(a) shows that when O_2 or N_2 are added to the discharge, the etch rate of the Si substrate increases. Second, if O_2 is added to the discharge, the etch rate of silicon increases more than if the same amount of N_2 is added. Figure 11(b) shows again that the etch rate decreases with increasing steady-state fluorocarbon film thickness. These results are consistent with the mechanism in which fluorocarbon deposition, fluorocarbon etching and substrate etching need to be balanced. The fluorocarbon deposition rate is found to be relatively constant for the investigated conditions compared to the large changes in Si and fluorocarbon etch rates. The fluorocarbon etch rate increases significantly both with O_2 and N_2 addition and the increase is larger if a given amount of O_2 rather than N_2 is added. The increase in fluorocarbon etch rate is consistent with the suggested role for substrate oxygen and nitrogen to assist in the carbon consumption. The result that the increase in fluorocarbon etch rate is larger for a certain amount of added O_2 than N_2, however, does not necessarily mean that atomic oxygen is more reactive than nitrogen, since N_2 is more difficult to dissociate than O_2.[41]

C. Further validation of the mechanism

The above suggested mechanism implies that in a case where no fluorocarbon deposition occurs, there should not be a significant substrate chemistry dependence of the etch characteristics. It is already observed that for low deposition rates, Si_3N_4 and SiO_2 etching are relatively close. In the case of no fluorocarbon deposition at all, Si should follow the Si_3N_4 in its behavior to etch similarly to oxide.

In order to validate this implication of the suggested mechanism, a set of Si etch experiments in C_2F_6 discharges was performed. The operating pressure was varied from 6 to 20 mTorr, the total gas flow ranged from 10 to 40 sccm, and the inductive power level was adjusted from 600 to 1400 W. The rf bias power was varied such that the self-bias voltage was kept at −100 V for all conditions. At high pressures and low inductive power the plasma conditions were such that no net fluorocarbon deposition occurs at 0 W rf bias power.

Figure 12(a) shows the measured Si etch rates for this set of data as a function of fluorocarbon film thickness. The general trend of decreasing etch rate with increasing fluorocarbon film thickness is still observed, but there is a great deal of scatter, especially for small fluorocarbon film thickness. However, the ion density varies significantly across the investigated parameter space. To correct for the changes in ion density it is more useful to plot the experimental results in terms of etch yield, i.e., number of substrate atoms removed per incident ion. Figure 12(b) shows the etch yields, calculated by using values for the ion current densities measured with a Langmuir probe, as a function of the fluorocarbon film thickness. For a clean Si substrate it is found that the etch yield is around 1.5 atoms per ion, and the etch yield decreases exponentially with fluorocarbon film thickness. When converting the oxide etch rates in Fig. 6 to etch yields we find values in the range of 0.67–0.86. These values are close to the values measured on Si covered with a fluorocarbon film that has a thickness in the range of 0.5–1 nm. Small discrepancies between Si and SiO_2 etch yields of fluorocarbon ions are to be expected. The results shown here clearly

support the above suggested general fluorocarbon etch mechanism in which the key step is to control the steady-state fluorocarbon film thickness. The fact that the etch yield rather than the rate is controlled by the fluorocarbon film thickness indicates that each individual ion contributes directly to the etch process, either by dissipating its energy or by providing the system with fluorine (e.g., through ion impact dissociation or fluorine liberation in the fluorocarbon film).

D. Mathematical description

The essence of the above mechanism can be captured in a simple set of equations. It was suggested that the amount of fluorocarbon material on a surface is a result from a complex balance between fluorocarbon deposition, fluorocarbon etching and substrate etching, which can aid in fluorocarbon removal. This balance can be written as

$$\frac{d}{dt}d(t) = DR_{\mathrm{CF}_x} - ER_{\mathrm{CF}_x} - CR_{\mathrm{CF}_x}, \tag{4}$$

where d is the fluorocarbon thickness, DR_{CF_x} is the fluorocarbon deposition rate during etching, ER_{CF_x} is the total fluorocarbon etch rate due to the plasma, and CR_{CF_x} is the fluorocarbon consumption rate due to substrate etching.

The fluorocarbon consumption rate CR_{CF_x} will be proportional to the substrate etch rate and therefore be dependent on the fluorocarbon film thickness on the surface. Fig. 6 showed that the substrate etch rate dependence decreases exponentially with fluorocarbon film thickness, i.e.,

$$ER_{\mathrm{sub}} = ER_0 \exp(-d/\lambda), \tag{5}$$

where ER_0 is a proportionality constant, which symbolizes the etch rate of a clean surface, and λ is a typical attenuation length for energy dissipation and fluorine concentration and estimated from Fig. 6 to be around 1 nm. The fluorocarbon consumption rate can thus be written as follows:

$$CR_{\mathrm{CF}_x} = CR_0 \exp(-d/\lambda), \tag{6}$$

where CR_0 is a proportionality constant that in fact symbolizes the rate at which fluorocarbon material is consumed if the substrate keeps itself clean during etching.

Next to the carbon removal rate due to substrate etching, the total fluorocarbon etch rate due to the plasma ER_{CF_x} in Eq. (4) can be assumed to have a thickness dependence. In the etching of semi-infinitely thick fluorocarbon films, e.g., fluorocarbon films deposited at 0 W rf bias power, all dissipated energy and atomic fluorine will be used to remove the fluorocarbon material. When the fluorocarbon film is thin enough, some of the ion bombardment energy will be dissipated in the substrate material instead of the fluorocarbon film. The etching of the fluorocarbon film will be reduced since the available fluorine and energy has to be shared with the substrate etching process. Figure 6 showed that the amount of energy or fluorine used for substrate etching, increases exponentially with decreasing fluorocarbon film thickness. If it is assumed that the exponential dependence holds for the fluorocarbon material, the fluorocarbon etch rate can be written as

$$ER_{\mathrm{CF}_x} = ER_\infty(1 - \exp(-d/\lambda)), \tag{7}$$

where ER_∞ is a proportionality constant that symbolizes the total fluorocarbon etch rate by the plasma when etching a semi-infinitely thick fluorocarbon film. In order to find ER_∞ for the different process conditions, it needs to be expressed in measurable values. This is done by writing Eq. (4) for etching a semi-infinitely thick fluorocarbon film:

$$\frac{d}{dt}d = DR_{\mathrm{CF}_x} - ER_\infty = ER_{\mathrm{net}}, \tag{8}$$

where ER_{net} is the net change in fluorocarbon thickness per time, which can be measured by ellipsometry. ER_{net} was referred to in the section experimental results as the fluorocarbon etch rate.

When solving the fluorocarbon balance for steady-state substrate etching conditions:

$$DR_{\mathrm{CF}_x} - ER_{\mathrm{CF}_x} - CR_{\mathrm{CF}_x} = 0, \tag{9}$$

one finds an expression in which the fluorocarbon film thickness depends on the fluorocarbon deposition rate DR_{CF_x}, the net fluorocarbon etch rate ER_{net} and the carbon consumption rate of a clean surface CR_0. Substituting the expression for the steady-state fluorocarbon film thickness in Eq. (5), gives the following expression for the substrate etch rate:

$$ER_{\mathrm{sub}} = \frac{ER_0}{1 + ((DR_{\mathrm{CF}_x} - CR_0)/ER_{\mathrm{net}})}. \tag{10}$$

This expression captures the observed experimental trends well. It clearly shows that in the case of Si etching where the substrate cannot aid in fluorocarbon removal, i.e., $CR_0 = 0$, the substrate etch rate is a function of both the fluorocarbon deposition DR_{CF_x} and net fluorocarbon etch rate ER_{net}. On the other hand, in the case of SiO_2 etching where the substrate consumes the majority of the deposited fluorocarbon material during etching reactions, i.e., $CR_0 \approx DR_{\mathrm{CF}_x}$, it is clear that the substrate etch rate is relatively independent of the fluorocarbon deposition DR_{CF_x} and fluorocarbon etch rate ER_{net}, and thus independent of the feedgas chemistry. In the case of Si_3N_4 etching, the substrate can only consume all deposited fluorocarbon material if the deposition rate is below a certain level. In other words, for relatively low fluorocarbon deposition rate $CR_0 \approx DR_{\mathrm{CF}_x}$, until CR_0 reaches its maximum and levels off. (Note: in the case of SiO_2 there will also be a maximum deposition rate that can be consumed. This maximum deposition rate apparently lies outside the investigated process regime, although in the case of C_3F_6 or C_3F_6/H_2 processing slight increases in the fluorocarbon film thickness on SiO_2 surfaces were already observed.)

It needs to be noted that the above rate equation describes the situation for a constant ion flux to the surface. In the previous section it was seen, however, that the etch yield rather than the etch rate depends on the fluorocarbon film

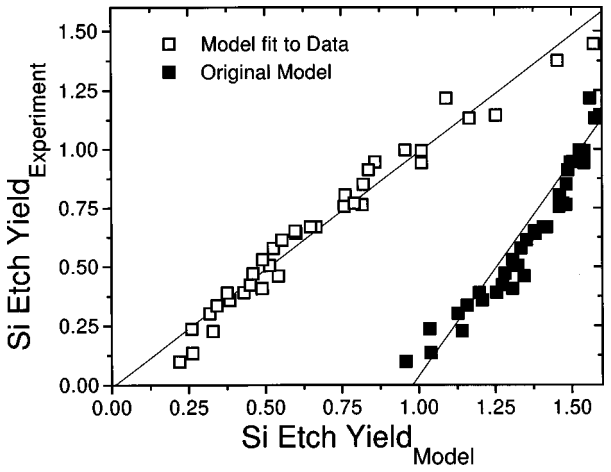

FIG. 13. Comparison between predicted etch yields and calculated etch yields. The solid points are calculated using the original model, the open points correspond to the calibrated model.

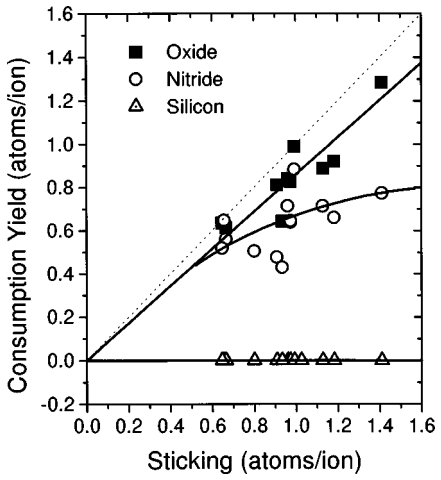

FIG. 14. Dependence of the carbon consumption yield for SiO_2, Si_3N_4, and Si on fluorocarbon sticking calculated for the data from Fig. 6 by comparing the SiO_2 and Si_3N_4 etch rates to Si. On the dotted line the consumption yield is equal to the sticking.

thickness. Equation (10), however, can directly be used to calculate the etch yields at a specific condition, provided that all rate parameters are converted into yield parameters. The proportionality constant ER_0 that symbolizes the etch rate of a clean substrate must thus be replaced by the etch yield (atoms removed per incident ion) of a clean substrate EY_0, the fluorocarbon deposition rate DR_{CF_x} is replaced by the sticking per incident ion S, the net fluorocarbon etch rate ER_{net} changes into the net fluorocarbon etch yield EY_{net}, and finally the fluorocarbon consumption rate CR_0 is converted to the consumption yield CY_0.

In order to quantitatively check the suggested model the fluorocarbon deposition rates and net fluorocarbon etch rates were determined for the same conditions as the Si etch experiments in Fig. 12. Figure 13 shows how the measured etch yields correlate to the calculated etch rates (Note: the fluorocarbon consumption yield $CY_0=0$ in these calculations, since the substrate material is Si.) Although the model qualitatively succeeds in predicting the Si etch yields, quantitative discrepancies exist. When a fit parameter f is introduced in the above model:

$$EY_{sub}=\frac{EY_0}{1+f\cdot((S-CY_0)/EY_{net})}, \tag{11}$$

quantitative agreement between the model and the experiments is found for a value of $f=9$. This value could partly be due to the fact that the actual fluorocarbon removal rate by the plasma is overestimated in Eqs. (7) and (8). It is conceivable that the ER_∞ value is lower for steady-state fluorocarbon films, that are deposited under conditions with highly energetic ion bombardment, than for fluorocarbon films deposited under 0 W rf bias conditions. Formation of hard and highly cross-linked films is possible under the actual etching conditions (Note: cross-linking does not necessarily change the average chemical composition observed by XPS analysis). Further, the actual fluorocarbon deposition rate/sticking per ion during substrate etching may be underestimated by taking it to be equal to the 0 W rf bias deposition rate/sticking. Enhanced implantation of fluorocarbon ions into the substrate during steady-state etching or additional creation of surface sites for neutral fluorocarbon deposition precursors may enhance the total fluorocarbon deposition.

The introduction of fit parameter f appears to be useful to calibrate the described model in its simplest form, i.e., for a Si substrate. We applied the model in its calibrated form to the data from Fig. 6, and determined the fluorocarbon consumption yields CY_0 for SiO_2 and Si_3N_4 at the various conditions. This can be done by comparing the SiO_2 and Si_3N_4 etch rates to the Si etch rates, while making the assumption that the etch yield of a clean surface EY_0 is similar for SiO_2, Si_3N_4, and Si substrates. This assumption is supported by the fact that the SiO_2, Si_3N_4, and Si data in Fig. 6 line up. Figure 14 shows the calculated consumption yield CY_0 as a function of atoms deposited per incident ion, i.e., sticking S, for the various materials. The consumption yield for Si is obviously equal to zero, since the model is calibrated in that fashion. The carbon consumption yield for SiO_2 is found to be close to the fluorocarbon sticking for all investigated conditions. The consumption yield for Si_3N_4 is only close to the fluorocarbon sticking if the fluorocarbon sticking is low. For higher sticking values, the consumption yield for Si_3N_4 levels off. The results in Fig. 14 nicely visualize that the fluorocarbon consumption ability of SiO_2 is such that it can keep its surface relatively clean of fluorocarbon material, while Si_3N_4 substrates can only consume fluorocarbon up to a certain level, resulting in the formation of relatively thick fluorocarbon films if the carbon supply is too large to be consumed.

V. CONCLUSIONS

Results of a study on selective SiO_2-to-Si_3N_4 etching in ICP discharges fed with different fluorocarbon gas mixtures (CHF_3, C_2F_6/C_3F_6, and C_3F_6/H_2) have been presented and

compared to selective SiO_2-to-Si etching. A general etch mechanism for SiO_2, Si_3N_4, and Si substrates has been formulated.

XPS surface analysis of SiO_2 and Si_3N_4 samples shows that a fluorocarbon film is present during steady-state etching conditions. The thickness of the film is strongly correlated with the etch rate of the substrate material. *The thicker the fluorocarbon film the lower the etch rate of the substrate material.* At the interface between the fluorocarbon film and the substrate material, a reaction layer is present. The thickness of this reaction layer decreases with increasing fluorocarbon film thickness, indicating that the fluorocarbon film protects the substrate from fluorine attack and therefore substrate etching.

The thickness of the fluorocarbon film is dependent on both the feedgas chemistry and the substrate material. SiO_2 films are covered with a relatively thin fluorocarbon film (<1.5 nm), while Si is covered with a relatively thick fluorocarbon film (2–7 nm). Si_3N_4 is intermediate between SiO_2 and Si (about 1–4 nm). The difference in film thickness on the various substrate materials is suggested to be due to a difference in the ability of a substrate material to consume carbon species from the fluorocarbon film in chemical reactions during substrate etching. The dependence of the fluorocarbon film thickness on the feedgas chemistry is suggested to be a result from a competition between fluorocarbon deposition, fluorocarbon removal, and substrate etching.

A mathematical description that includes the fluorocarbon deposition rate, net fluorocarbon etch rate, and a carbon consumption factor allows to predict trends in the substrate etch yields.

ACKNOWLEDGMENTS

The authors gratefully acknowledge support of this work by Lam Research Corporation, the New York State Science and Technology Foundation, and the Department of Energy under Contract No. DE-FG02-97ER54445. We would like to acknowledge R. J. Severens, M. C. M. v. d. Sanden, and D. C. Schram from Eindhoven University of Technology, and M. Chang and F. Wang from Advanced Micro Devices for helpful discussions. M. F. Doemling, B. E. E. Kastenmeier, and P. J. Matsuo are thanked for sharing the insights obtained in their parallel studies performed in the Plasma Processing and Research Laboratories at the University at Albany.

[1]R. A. H. Heinecke, Solid-State Electron. **18**, 1146 (1975).
[2]J. W. Coburn and E. Kay, IBM J. Res. Dev. **23**, 33 (1979).
[3]J. W. Coburn and H. F. Winters, J. Vac. Sci. Technol. **16**, 391 (1979).
[4]J. W. Coburn, J. Appl. Phys. **50**, 5210 (1979).
[5]L. M. Ephrath, J. Electrochem. Soc. **126**, 1419 (1979).
[6]Y.-Y. Tu, T. J. Chuang, and H. F. Winters, Phys. Rev. B **23**, 823 (1981).
[7]G. S. Oehrlein, G. J. Coyle, J. C. Tsang, R. M. Tromp, J. G. Clabes, and Y. H. Lee, Mater. Res. Soc. Symp. Proc. **68**, 367 (1986).
[8]G. S. Oehrlein and Y. H. Lee, J. Vac. Sci. Technol. A **5**, 1585 (1987).
[9]S. Joyce, J. G. Langan, and J. I. Steinfeld, J. Chem. Phys. **88**, 2027 (1988).
[10]J. G. Langan, J. A. Shorter, X. Xin, S. A. Joyce, and J. I. Steinfeld, Surf. Sci. **207**, 344 (1989).
[11]Ch. Cardinaud and G. Turban, Appl. Surf. Sci. **45**, 109 (1990).
[12]T. Akimoto, S. Furuoya, K. Harasima, and E. Ikawa, Jpn. J. Appl. Phys., Part 1 **33**, 2151 (1994).
[13]G. S. Oehrlein and H. L. Williams, J. Appl. Phys. **62**, 662 (1987).
[14]G. S. Oehrlein, S. W. Robey, and M. A. Jaso, Mater. Res. Soc. Symp. Proc. **98**, 229 (1987).
[15]G. E. Potter, G. H. Morrison, P. K. Charvat, and A. L. Ruoff, J. Vac. Sci. Technol. B **10**, 239 (1992).
[16]T. E. F. M. Standaert, M. Schaepkens, N. R. Rueger, P. G. M. Sebel, G. S. Oehrlein, and J. M. Cook, J. Vac. Sci. Technol. A **16**, 239 (1998).
[17]J. W. Butterbaugh, D. C. Gray, and H. H. Sawin, J. Vac. Sci. Technol. B **9**, 1461 (1991).
[18]N. R. Rueger, J. J. Beulens, M. Schaepkens, M. F. Doemling, J. M. Mirza, T. E. F. M. Standaert, and G. S. Oehrlein, J. Vac. Sci. Technol. A **15**, 1881 (1997).
[19]A. M. Barklund and H.-O. Blom, J. Vac. Sci. Technol. A **11**, 1226 (1993).
[20]J. Givens, S. Geissler, J. Lee, O. Cain, J. Marks, P. Keswick, and C. Cunningham, J. Vac. Sci. Technol. B **12**, 427 (1994).
[21]K. Ueno, T. Kikkawa, and K. Tokashiki, J. Vac. Sci. Technol. B **13**, 1447 (1995).
[22]H. Hayashi, K. Kurihara, and M. Sekine, Jpn. J. Appl. Phys., Part 1 **35**, 2488 (1996).
[23]S. Fang, C. Chiang, D. Fraser, B. Lee, P. Keswick, M. Chang, and K. Fung, J. Vac. Sci. Technol. A **14**, 1092 (1996).
[24]Y. Zhang, G. S. Oehrlein, and F. H. Bell, J. Vac. Sci. Technol. A **14**, 2127 (1996).
[25]J. M. Cook, O. Turmel, T. Wicker, and J. Winniczek, Technical Proceedings, Semicon Japan, SEMI, Chiba 1993 (unpublished), p. 414.
[26]F. H. Bell, O. Joubert, G. S. Oehrlein, Y. Zhang, and D. Vender, J. Vac. Sci. Technol. A **12**, 3095 (1994).
[27]J. H. Keller, J. C. Forster, and M. S. Barnes, J. Vac. Sci. Technol. A **11**, 2487 (1993).
[28]J. A. Meyer, K. H. R. Kirmse, J.-S. Jenq, S. Y. Perez-Montero, H. L. Maynard, A. E. Wendt, J. W. Taylor, and N. Hershkowitz, Appl. Phys. Lett. **64**, 1926 (1994).
[29]D. C. Marra and E. S. Aydil, J. Vac. Sci. Technol. A **15**, 2508 (1997).
[30]M. Haverlag, D. Vender, and G. S. Oehrlein, Appl. Phys. Lett. **61**, 2875 (1992).
[31]P. C. Zalm, *Handbook of Ion Beam Processing Technology*, edited by J. J. Cuomo, S. M. Rossnagel, and H. R. Kaufman (Noyes, NJ, 1989), p. 77; J. Kirschner and H. W. Etzkorn, Appl. Phys. A: Solids Surf. **29**, 133 (1982).
[32]S. W. Robey and G. S. Oehrlein, Surf. Sci. **210**, 429 (1989).
[33]J. A. Taylor, G. M. Lancaster, A. Ignatiev, and J. W. Rabalais, J. Chem. Phys. **68**, 1776 (1978).
[34]*Handbook of X-ray Photoelectron Spectroscopy*, edited by G. E. Muilenberg (Perkin-Elmer, Eden Prairie, MN, 1979).
[35]G. S. Oehrlein, J. Vac. Sci. Technol. A **11**, 34 (1993).
[36]N. Ikegami, N. Ozawa, Y. Miyakawa, and J. Kanamori, Jpn. J. Appl. Phys., Part 1 **30**, 1556 (1991); N. Ikegami, N. Ozawa, Y. Miyakawa, N. Hirashita, and J. Kanamori, **31**, 2020 (1992).
[37]J. Ding, J.-S. Jenq, G.-H. Kim, H. L. Maynard, J. S. Hamers, N. Herskowitz, and J. W. Taylor, J. Vac. Sci. Technol. A **11**, 1283 (1993).
[38]D. Field, D. F. Klemperer, and I. T. Wade, J. Vac. Sci. Technol. B **6**, 551 (1988).
[39]J. Dulak, B. J. Howard, and Ch. Steinbruechel, J. Vac. Sci. Technol. A **9**, 775 (1991).
[40]K. Miyata, M. Hori, and T. Goto, J. Vac. Sci. Technol. A **15**, 568 (1997).
[41]Y. Wang, R. J. Van Brunt, and J. K. Olthoff, J. Appl. Phys. **83**, 703 (1998).